Master of Science Thesis

Hybrid Eulerian-Lagrangian Vortex Particle Method

A fast and accurate numerical method for 2D Vertical-Axis Wind Turbine

L. Manickathan B.Sc.

Date TBD

Faculty of Aerospace Engineering · Delft University of Technology

Hybrid Eulerian-Lagrangian Vortex Particle Method

A fast and accurate numerical method for 2D Vertical-Axis Wind Turbine

Master of Science Thesis

For obtaining the degree of Master of Science in Aerospace Engineering at Delft University of Technology

L. Manickathan B.Sc.

Date TBD

Faculty of Aerospace Engineering · Delft University of Technology

Delft University Of Technology
Department Of
Aerodynamics and Wind Energy

The undersigned hereby certify that they have read and recommend to the Faculty of Aerospace Engineering for acceptance a thesis entitled **"Hybrid Eulerian-Lagrangian Vortex Particle Method"** by **L. Manickathan B.Sc.** in partial fulfillment of the requirements for the degree of **Master of Science**.

Dated: Date TBD

Head of department:	______________________ prof.dr.ir. G.J.W. van Bussel
Academic Supervisor:	______________________ dr.ir. C.J. Simao Ferreira
Academic Supervisor:	______________________ dr.ir. A. Palha da Silva Clerigo
Industrial Supervisor:	______________________ prof.dr.ir. I. Bennett

Summary

This is the summary of the thesis.

Acknowledgements

I wish to thank the following persons…

Delft, The Netherlands L. Manickathan B.Sc.
Date TBD

Contents

Summary v

Acknowledgements vii

List of Figures xiii

List of Tables xv

Nomenclature xvii

1 Introduction 1
- 1.1 Motivation and Goal . . . 1
- 1.2 Research Aim and Plan . . . 2
- 1.3 Introduction to Hybrid Eulerian-Lagrangian Vortex Particle Method . . . 2
  - 1.3.1 Advantage of domain decomposition . . . 2
  - 1.3.2 Methodology . . . 2
- 1.4 Thesis Outline . . . 2

2 Lagrangian Domain: Vortex Particle Method 3
- 2.1 Introduction to Vortex Particle Method . . . 3
  - 2.1.1 Vorticity . . . 3
  - 2.1.2 Velocity-vorticity formulation of the Navier-Stokes equations . . . 4
  - 2.1.3 Viscous splitting algorithm . . . 4
- 2.2 Spatial Discretization: Generation of Vortex Blobs . . . 5
  - 2.2.1 Biot-Savart law . . . 5
  - 2.2.2 Discrete form of vorticity field . . . 6
  - 2.2.3 Convection of vortex blobs . . . 6
  - 2.2.4 Mollified vortex kernels . . . 6
  - 2.2.5 Vortex blob initialization . . . 8

2.2.6 Remeshing scheme: Treating lagrangian grid distortion 11
2.3 Diffusion of Vortex Methods 13
2.3.1 Modified remeshing for treating diffusion 14
2.4 Boundary conditions at solid boundary 15
2.4.1 Boundary integral equations 17
2.4.2 Panel method for treating no-slip boundary condition 17
2.4.3 Convergence study of panel method 17
2.5 Simulation acceleration techniques 17
2.5.1 Fast multi-pole Method 17
2.5.2 Parallel computation in GPU 17
2.6 Validation of lagrangian method 17
2.6.1 Lamb-oseen vortex at $Re = 100$ 17
2.6.2 Convergence study of the viscous vortex method 17
2.6.3 Convection of Clercx-Bruneau dipole at $Re = 625$ 17
2.7 Summary 17

3 Eulerian Domain: Finite Element Method 19
3.1 Introduction to Finite Element Method 20
3.1.1 Finite element discretization 20
3.1.2 Finite element function and function space 20
3.2 Solving the Finite Element problem 20
3.2.1 Introduction to FEniCS Project 20
3.2.2 Mesh generation using GMSH 20
3.3 Solving Incompressible Navier-Stokes Equations 20
3.3.1 Velocity-pressure formulation 20
3.3.2 Incremental pressure correction scheme 20
3.3.3 Determining the vorticity field 20
3.3.4 Determining the body forces 20
3.4 Validation of eulerian method 20
3.4.1 Clercx-Bruneau dipole collison at $Re = 625$ 20
3.4.2 Impulsively started cylinder at $Re = 550$ 20
3.5 Summary 20

4 Hybrid Eulerian-Lagrangian Vortex Particle Method 21
4.1 Theory of Domain Decomposition Method 21
4.1.1 Advantage of domain decomposition 21
4.1.2 Assumptions and Limitations 21
4.1.3 Modified coupling strategy 21
4.2 Eulerian-Lagrangian coupling algorithm 21
4.2.1 Eulerian dirichlet boundary condition 21
4.2.2 Vorticity interpolation algorithm 21
4.3 Introduction to pHyFlow: Hybrid solver 21
4.3.1 Program structure 21
4.4 Summary 21

5 Verification and Validation of Hybrid Method 23
5.1 Error in coupling: Verification with Lamb-Ossen vortex . . . 24
5.1.1 Generation of artificial vorticity . . . 24
5.2 Clercx-Bruneau dipole convection at $Re = 625$ . . . 24
5.2.1 Comparison of vorticity contours . . . 24
5.2.2 Variation in maximum vorticity . . . 24
5.2.3 Variation in kinetic energy . . . 24
5.2.4 Variation in enstrophy . . . 24
5.3 Clercx-Bruneau dipole collison at $Re = 625$ . . . 24
5.3.1 Comparison of vorticity contours . . . 24
5.3.2 Variation in maximum vorticity . . . 24
5.3.3 Variation in kinetic energy . . . 24
5.3.4 Variation in enstrophy . . . 24
5.3.5 Variation in palinstrophy . . . 24
5.4 Impulsively started cylinder problem at $Re = 550$ . . . 24
5.4.1 Evolution of the wake . . . 24
5.4.2 Evolution of pressure and friction drag . . . 24
5.4.3 Evolution of lift . . . 24
5.5 Moving body . . . 24
5.5.1 Error due to pertubation lag . . . 24
5.6 Proof of concepts . . . 24
5.6.1 Multiple cylinder case . . . 24
5.6.2 Stalled airfoil at $Re = 5000$ . . . 24
5.7 Summary . . . 24

6 Conclusion and Recommendation 25
6.1 Conclusion . . . 25
6.1.1 Lagrangian domain . . . 25
6.1.2 Eulerian domain . . . 25
6.1.3 Hybrid method . . . 25
6.2 Recommendations . . . 25
6.2.1 Lagrangian domain . . . 25
6.2.2 Eulerian domain . . . 25
6.2.3 Hybrid method . . . 25

References 27

List of Figures

2.1 Circulation of the fluid . . . 4

2.2 Vortex blob with Gaussian distribution: [$k = 2$, $\sigma = 1.0$] . . . 7

2.3 Vortex blob with overlap σ/h . . . 8

2.4 Mollified vorticity field of an arbitrary vorticity function with overlap = 1.0, $\sigma = 0.19$, $h = 0.19$. Vortex blob strength has been assigned by equation 2.20, sampling at exact vorticity [•, red dot]. Figure depicts exact vorticity distribution ω [—, solid], vorticity field of each blob ω_i [—, green dashed], the mollified vorticity field ω^h [- -, dashed]. . . . 9

2.5 Mollified vorticity field after two Beale's iteration, overlap = 1.0, $\sigma = 0.19$, $h = 0.19$. Figure depicts exact vorticity distribution ω [—, solid], vorticity field of each blob ω_i [—, green dashed], the mollified vorticity field ω^h [- -, dashed]. . . . 10

2.6 Convergence of vorticity by modifying the spatial resolution. Figure depicts exact vorticity field ω with [—, black] and various resolutions. . . . 10

2.7 Lagrangian distortion of the vortex blobs after 100 steps. The initial vorticity field $\omega(\mathbf{x}, 0) = \exp(-12\,|\mathbf{x}|)$ with $\Delta t = 0.1$, $\sigma = 0.02$ and overlap = 1.0. Figure depicts the initial and the final distribution of the vortex blobs. . . . 11

2.8 Interpolation of vortex blob (•, green) on the uniform grid. . . . 12

2.9 Interpolation kernel . . . 13

2.10 Extended vorticity field consisting of vorticity in the fluid and vortex sheet distribution. . . . 16

2.11 Extended vorticity field: Vortex blobs and Vortex sheets . . . 16

List of Tables

Nomenclature

Latin Symbols

c^2	Diffusion parameter	$[-]$
$\mathcal{E}$	Enstrophy	$[m^2 \cdot s^{-2}]$
h	Nominal particle spacing	$[m]$
h_ν	Diffusion distance	$[m]$
$\mathbf{K}$	Biot-Savart kernel	$[-]$
$\mathbf{K}_\sigma$	Vortex blob kernel	$[-]$
N_p	Number of particles	$[-]$
overlap	Overlap ratio of the blobs	$[-]$
p	Pressure	[Pa]
t	Time	$[s]$
$\mathbf{u}$	Velocity	$[m \cdot s^{-1}]$
$\mathbf{u}^h$	Discrete velocity	$[m \cdot s^{-1}]$
$\mathbf{u}_\infty$	Free-stream velocity	$[m \cdot s^{-1}]$
$\mathbf{u}_\phi$	Potential velocity	$[m \cdot s^{-1}]$
$\mathbf{u}_\omega$	Vortical velocity	$[m \cdot s^{-1}]$
W	Interpolation kernel weight	$[-]$
$\mathbf{x}$	Position vector	$[m]$
$\mathbf{x}_p$	Position vector of the particle	$[m]$

Greek Symbols

α_p	Circulation of the particle	$[m^2 \cdot s^{-1}]$
β_p	Corrected circulation of the particle	$[m^2 \cdot s^{-1}]$
Δt_c	Convection time-step size	$[s]$
Δt_d	Diffusion time-step size	$[s]$
ϵ	Distance between the particles	$[m]$
ζ_σ	Smooth cut-off function of the blob	$[-]$
Γ	Circulation	$[m^2 \cdot s^{-1}]$
ν	Kinematic viscosity	$[m^2 \cdot s^{-1}]$
ρ	Density	$[kg \cdot m^{-3}]$
σ	Core size	$[m]$
ω	Vorticity	$[s^{-1}]$
ω^h	Discrete vorticity field	$[s^{-1}]$

Abbreviations

FMM	Fast-Multipole Method
GPU	Graphics Processing Units
PSE	Particle Strength Exchange
VAWT	Vertical-Axis Wind Turbine
VPM	Vortex Particle Method
VRM	Vortex Redistribution Method

Chapter 1

Introduction

Conventional energy resources such as fossil fuels and nuclear energy are not only limited supply but also pose adhere effects on the environment. Therefore, we are striving to find a cheap and renewable source of energy. Wind energy is such source of energy and is therefore getting more popular and also become more affordable and novel renewable technologies such as Vertical-Axis Wind Turbine (VAWT) is now an interested research field.

Vertical-Axis Wind turbines are unlike the normal wind turbine. Typical wind turbines are mounted on a mast away from the ground and generates energy by spinning normal to the ground. However, a VAWT spins parallel to the ground with its hub located at the ground [14]. The advantages of the vertical axis wind turbine are what makes them ideal for a source of renewable energy. As the turbine is located at the ground (unlike the Horizontal-Axis Wind Turbine), it is easily accessible and can be easily maintained. The second main advantage of the VAWT is the way it dissipates its wake [6] [12]. As the fluid past the turbine is more turbulent, the flow is able to smooth out much earlier. This means that it possible to places VAWTs much closer to each other is so in future this means that a VAWT farm can potentially give more power per area. Furthermore, operate independent of the flow direction and can operate at low wind speeds (low tip-speed ratios).

1.1 Motivation and Goal

However, with these advantages also comes drawbacks. As the blades passes through its own dirty air (the wake), complex wake-body interactions take places. These have adhere effect on the blade structure and therefore is more susceptible to fatigue. This happens because the blades are constantly pitching in front the free-stream flow and complex flow behaviour such as dynamic stall and constant vortex shedding occurs [10]. This complex fluid behaviours makes it hard to predict the performance of a VAWT and this is one of the reasons why VAWTs are not mainstream. In addition, as the VAWT operates at large Reynolds number, accurate numerical methods are computationally very expensive. Therefore, it is vital to have a good understanding of the flow structure evolution and the wake generation of the VAWT using not only an efficient method, but also an accurate one.

To summarize, we are now able to formulate a research goal. The key interest of this project is to develop an efficient, reliable, and an accurate numerical method for modelling the flow around a 2D VAWT. For now, only 2D problems are considered because 3D method is build upon the methodology of the 2D. Thus, once the 2D methodology is made, a 3D numerical method should be a straightforward extension.

Furthermore, the numerical method efficient at capturing both the near-wake phenomenons such as the vortex shedding, dynamic stall, & the wake-body interaction, and should be able to capture the large scale flow structure such as the evolution of the VAWT wake. From this criterias, we are able to formulate the research question.

1.2 Research Aim and Plan

Research Question: *Is it possible to develop a numerical method that is both efficient at capturing the small-scale phenomenons and the large scale phenomenons? Is is possible to apply this to a 2D VAWT?*

Research aim and plan:

- Develop a numerical method for capturing small-scale phenomenons and large scale phenomenons.
- Ensure this tool is efficient, reliable, and accurate.
- Verify, Validate the tools with model problems.
- Apply the model to the 2D flow of VAWT.

With the above formulate research question, aim and plan we are able to thoroughly perform the literature study to determine whether the research goal stated here is feasible. Finally, this report will answer why a Hybrid Eulerian-Lagrangian Vortex Particle Method will be used to the achieved the goals.

1.3 Introduction to Hybrid Eulerian-Lagrangian Vortex Particle Method

1.3.1 Advantage of domain decomposition

1.3.2 Methodology

1.4 Thesis Outline

Chapter 2

Lagrangian Domain: Vortex Particle Method

2.1 Introduction to Vortex Particle Method

Vortex Particle Method (VPM) is a branch of computational fluid dynamics that deals with the evolution of the vorticity of the fluid in a lagrangian description. Typically, the fluid is viewed at a fixed window where it is described as a function of space $\mathbf{x}$ and time t. However, the lagrangian point of view regards the fluid as a collection of the particles carrying the property of the fluid.

Unlike the typical eulerian method that require discretization of all the fluid domain, VPM only needs fluid elements where there is vorticity. This means that the VPM are inherently auto-adaptive method that only simulated the flow of interest. Furthermore, with the computational acceleration methods such as Fast-Multipole Method (FMM) and parallel computation on Graphics Processing Units (GPU) , VPM can be more efficient that typical eulerian methods.

2.1.1 Vorticity

Vorticity ω, the governing element of vortex particle method, is defined as

$$\omega = \Delta \times \mathbf{u}, \tag{2.1}$$

where $\mathbf{u}$ is the velocity. The circulation Γ is defined as

$$\Gamma = \int_L \mathbf{u} \cdot d\mathbf{r} = \int_S \omega \cdot \mathbf{n} \, dS, \tag{2.2}$$

by the stokes theorem, as represents the integral vorticity of the domain, figure 2.1

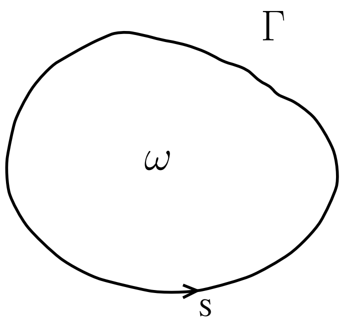

Figure 2.1: Circulation of the fluid

2.1.2 Velocity-vorticity formulation of the Navier-Stokes equations

The governing equation of the vortex particle method is velocity-vorticity $\mathbf{u} - \omega$ formulation of the Navier-Stokes equations [4]. The 2-D incompressible Navier-Stokes momentum equation is given as

$$\frac{\partial \mathbf{u}}{\partial t} + \mathbf{u} \cdot \nabla \mathbf{u} = -\frac{1}{\rho} \nabla p + \nu \nabla^2 \mathbf{u}, \tag{2.3}$$

relating the velocity field $\mathbf{u}(\mathbf{x}, t)$ to the pressure field $\mathbf{p}(\mathbf{x}, \mathbf{t})$, the kinematic viscosity ν and density ρ. Furthermore, we also have to satisfy the incompressibility constraint given as

$$\nabla \cdot \mathbf{u} = 0. \tag{2.4}$$

To attain the velocity-vorticity formulation, we should take the curl of the velocity-pressure $\mathbf{u} - p$ formulation of the Navier-Stokes equation. Taking the curl of the momentum equation 2.3, we get the vorticity transport equation

$$\frac{\partial \omega}{\partial t} + \mathbf{u} \cdot \nabla \omega = \nu \nabla^2 \omega, \tag{2.5}$$

which only relates the vorticity to the velocity enabling us to neglect the pressure field. Note that as we are dealing with the two dimensional flow, we neglected the stretching term.

2.1.3 Viscous splitting algorithm

Vortex particle method was initially used to model the evolution of incompressible, inviscid flows. However, in order to simulate a real flow, we must also deal with the viscous behaviour of the fluid. Chorin [3] has shown that using the viscous splitting algorithm, it is possible to simulate a viscous flow.

The viscous splitting algorithm is basically a fractional step method, where the viscous and the inviscid part of the transport equation is dealt in two subsequent steps,

- Sub-step 1: convection

$$\frac{\partial \omega}{\partial t} + \mathbf{u} \cdot \nabla \omega = 0; \tag{2.6}$$

- Sub-step 2: diffusion

$$\frac{\partial \omega}{\partial t} = \nu \nabla^2 \omega. \tag{2.7}$$

The first sub-step of the evolution deals with the convection of the vorticity. Note that, by convection we imply the advection of the vorticity field where the diffusion process is neglected. The second sub-step is where we deals with the diffusion of the vorticity field.

There are several advantage to this type of evolution. As the convection and diffusion are handled separately, there is minimum dispersion during the convection and furthermore, the is no restriction of the advection CFL number [13].

There are many ways of dealing with the diffusion of the vorticity field. During this project, we use a modified interpolation kernel [13] that can simultaneously treat diffusion and remesh the vortex particles, see section 2.3.

2.2 Spatial Discretization: Generation of Vortex Blobs

In order to deal with the vorticity field, we must first discretize the vorticity to vortex particles. Vortex blobs have been first introduced by Chorin and is a mollified particle carrying the local circulation. Vortex blobs describes a smooth vorticity field and are ideal because of it does not cause singularity issues when particles approach each other.

!!! check for consistency, continuity !!!

2.2.1 Biot-Savart law

The velocity field can be decomposed using the Helmholtz decomposition, given as

$$\mathbf{u} = \mathbf{u}_\omega + \mathbf{u}_\phi, \tag{2.8}$$

where $\mathbf{u}_\omega$ is the rotational component of the velocity and $\mathbf{u}_\phi$ is the irrotational component. solenoidal and potential velocity respectively. In an unbounded flow we have $\mathbf{u}_\phi$ equal to the free-stream velocity $\mathbf{u}_\infty$. For bounded flow, we must include the presence of the body, see section 2.4.

The velocity can be related to the vorticity using the Biot-Savart law

$$\mathbf{u}_\omega = \mathbf{K} \star \omega, \tag{2.9}$$

where the $\star$ represents convolution of the 2-D kernel $\mathbf{K}$ given by

$$\mathbf{K} = \frac{1}{2\pi \left|\mathbf{x}\right|^2} \left(-x_2, x_1\right). \tag{2.10}$$

2.2.2 Discrete form of vorticity field

The spatial discretization of the fluid domain is done through N quadrature points. With the Biot-Savart law, we can treat these quadratures are discrete particles carrying the local quantities. The discrete vorticity field is given as

$$\omega\left(\mathbf{x},t\right) \simeq \omega^{h}\left(\mathbf{x},t\right) = \sum_{p} \alpha_{p}\left(t\right) \delta\left[\mathbf{x} - \mathbf{x}_{p}\left(t\right)\right], \tag{2.11}$$

where α_p is the estimate of the circulation around the particle $\mathbf{x}_p$ with core size σ. We must not that ω^h is an approximately equal to ω of the fluid due to the discretization.

The discrete form of the velocity is therefore written as

$$\mathbf{u} \simeq \mathbf{u}^{h} = \sum_{p} \mathbf{K}\left[\mathbf{x} - \mathbf{x}_{p}\left(t\right)\right] \alpha_{p}\left(t\right). \tag{2.12}$$

Thus the discrete vorticity field is an N-body problem inducing velocity on each and implicitly evolving the vorticity field. This is one of the advantage of the vortex particle method as there are many ways to efficiently treat the problem. The N-body problem can be parallelized and can be accelerated using fast summation methods such as FMM, see 2.5.

However, like all N-body problem, equation 2.10 has a singularity when the particles approach each other and can result in numerical instability. To overcome this we can mollify the kernel, removing the singularity.

2.2.3 Convection of vortex blobs

In the discrete of the convection equation 2.6 of the viscous-splitting algorithm, the is solved as system of ODEs, where

$$\frac{\mathrm{d}\mathbf{x}_p}{\mathrm{d}t} = \mathbf{u}\left(\mathbf{x}_p\right), \tag{2.13}$$

with

$$\frac{\mathrm{d}\alpha_p}{\mathrm{d}t} = 0. \tag{2.14}$$

As the diffusion is done at the next sub-step, we have to ensure that the circulation is conserved.

2.2.4 Mollified vortex kernels

A vortex particle with a mollified core, non-zero core-size, is referred to as vortex blobs. The advantage of the vortex blobs is that the with a smooth distribution of the vorticity, the singularity disappears and so numerical instability does not happen when blobs get too close to each other. An ideal choice for a cutoff function is a Gaussian distribution, figure 2.2.

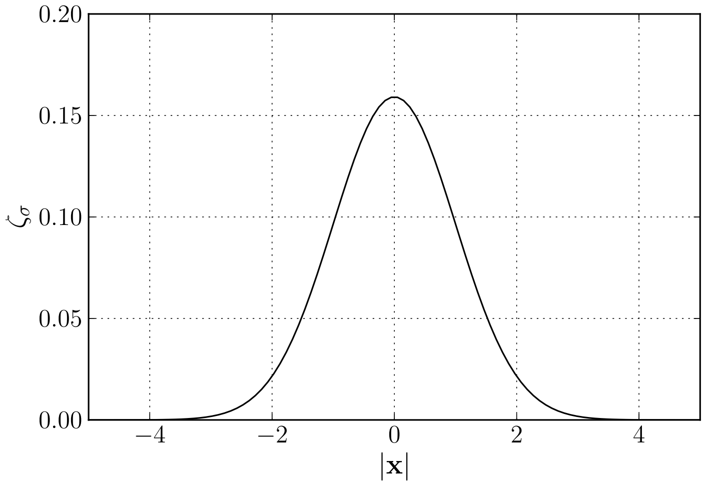

Figure 2.2: Vortex blob with Gaussian distribution: $[k = 2,\ \sigma = 1.0]$

Gaussian kernels satisfy the requirement for smooth distribution ad decays quickly and is defined as

$$\zeta_\sigma = \frac{1}{k\pi\sigma^2} \exp\left(\frac{-|\mathbf{x}|}{k\sigma^2}\right), \tag{2.15}$$

where k is 1, 2 or 4 and determines the width of the kernel, σ is core-size of the blob. Note that smoothing function is chosen such that $\int \zeta = 1$, ensuring the conservation of circulation when mollified. So, using a smooth cut-off function ζ_σ, the mollified kernel $\mathbf{K}_\sigma$ is given as

$$\mathbf{K}_\sigma = \mathbf{K} \star \zeta_\sigma. \tag{2.16}$$

The mollified vorticity field, represented by vortex blobs is given as

$$\omega^h(\mathbf{x}, t) = \sum_p \alpha_p(t)\, \zeta_\sigma\left[\mathbf{x} - \mathbf{x}_p(t)\right], \tag{2.17}$$

now representing the mollified vorticity field and equivalently, the mollified velocity field is given as

$$\mathbf{u}^h(\mathbf{x}, t) = \sum_p \mathbf{K}_\sigma\left[\mathbf{x} - \mathbf{x}_p(t)\right] \alpha_p(t). \tag{2.18}$$

Koumoutsakos and Chorin [4], have shown that for proper communication between the particle, the particle needs to overlap,

$$\text{overlap} = \frac{\sigma}{h}, \tag{2.19}$$

where h is the nominal particle spacing, figure 2.3. If the particles fail to overlap, vortex blobs will also fail to recover the vorticity field. Such problems occurs when blobs are clustered due to high flow strain, leading to lagrangian grid distorting and must be treated, see section 2.2.6.

2.2.5 Vortex blob initialization

Now the question arises on how to initialize the particle's circulation strengths α_p. A common approach that is used is to estimate the particles strength is to say that

$$\alpha_p = \omega_p \cdot h^2. \tag{2.20}$$

This might seem like a valid assumption as the circulation of a given area is the integral of the vorticity in the area, equation 2.2, however this is no longer valid when regularizing the vorticity field using mollified gaussian kernels, equation 2.17. Barba and Rossi [1], has described this problem as gaussian blurring of the original vorticity field. Even though the particle have acquired the correct circulation strengths (i.e the local property), when evaluating the mollified vorticity field, we see that there is a mismatch in the evaluated vorticity field, figure 2.4.

Another way of viewing this characteristic is say the conservation of circulation is only valid globally, but not locally. A common standard for recovering the initial vorticity field is perform the Beale's method [2].

Beale's Iterative Method

The Beale's method is particle circulation processing scheme where the circulation of the particles are modified such that the mollified vorticity field matches the indented vorticity field. The recovery of the vorticity field is done by performing a discrete deconvolution,

$$\sum_{j}^{N} \beta_j \zeta_\sigma \left(\mathbf{x}_i - \mathbf{x}_j\right) = \omega_i, \tag{2.21}$$

where β_j is the circulation of the particles at positions $\mathbf{x}_j$ such that it matches the exact vorticity ω_i at the position $\mathbf{x}_i$ that we are evaluating. As we are try to solve for a N

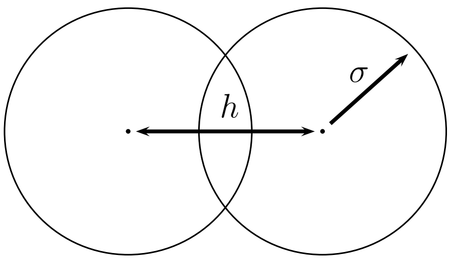

Figure 2.3: Vortex blob with overlap σ/h

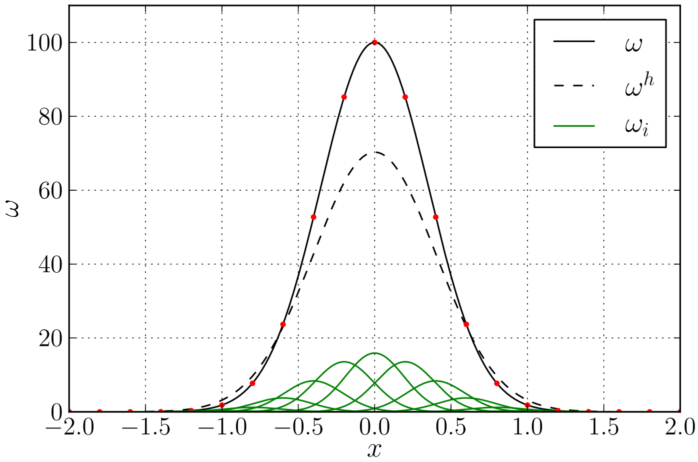

Figure 2.4: Mollified vorticity field of an arbitrary vorticity function with overlap $= 1.0$, $\sigma = 0.19$, $h = 0.19$. Vortex blob strength has been assigned by equation 2.20, sampling at exact vorticity [•, red dot]. Figure depicts exact vorticity distribution ω [—, solid], vorticity field of each blob ω_i [—, green dashed], the mollified vorticity field ω^h [- -, dashed].

unknown problem, we must set up a N system of equations. Multiplying both sides with the area associated to the blobs, we get

$$\mathbf{A}_{ij}\beta_j = \alpha_i^{\text{exact}}, \tag{2.22}$$

where

$$\mathbf{A}_{ij} = \zeta_\sigma\left(\mathbf{x}_i - \mathbf{x}_j\right) \cdot h^2 \tag{2.23}$$

is a $N \times N$ matrix containing the weights of the influence of each particle on each other. This matrix can be constructed by setting the Γ to one and determine the induced vorticity on each other. Furthermore, we see that it is not feasible to directly invert the matrix when we have large set of blobs but most importantly as the matrix $\mathbf{A}$ is severly ill-conditioned [11], it should not be directly inverted. Beale's proposition to this problem was to iteratively solve for the solution,

$$\beta_j^{n+1} = \alpha_i + \beta_i^n - \mathbf{A}_{ij} \cdot \beta_j^n \tag{2.24}$$

We see that with just two iterations, the error between the mollified and exact vorticity field reduces drastically, figure 2.5. Koumoutsakos and Cottet [4], had shown that there was a drastic improvement in the velocity with just two to three iterations. However, we see that the cell vorticity of the blobs, directly evaluated from the particle strengths, equation 2.20, are more peaky and no longer matches the exact vorticity.

During the hybrid coupling algorithm, we see that this is the central source of coupling error between the eulerian and the lagrangian method, section **??**. When performing the hybrid coupling, we need to recover the vorticity field transfered from the eulerian domain

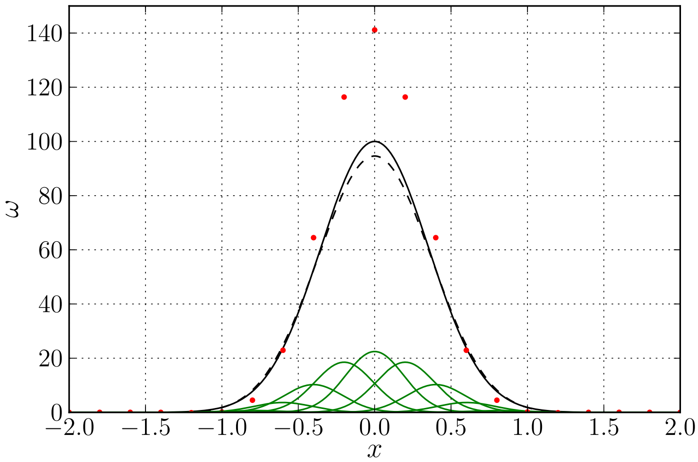

Figure 2.5: Mollified vorticity field after two Beale's iteration, overlap $= 1.0$, $\sigma = 0.19$, $h = 0.19$. Figure depicts exact vorticity distribution ω [—, solid], vorticity field of each blob ω_i [—, green dashed], the mollified vorticity field ω^h [- -, dashed].

to the lagrangian domain in every step. So, beale's correction is not a viable solution for the hybrid method. Thus there is a need for an alternate method of recovering the vorticity field.

!!! add the reference to hybrid !!!

Convergence of particle discretization

An alternate, temporary method to reduce the gaussian blurring of the vorticity field is to reduce the overlap (i.e. increase the overlap ratio) of the vortex blobs and to the increase the spatial resolution.

Figure 2.6 shows mollified vorticity field results from modifying the spatial resolution parameters. Figure 2.6a shows the convergence of the mollified vorticity field ω^h to

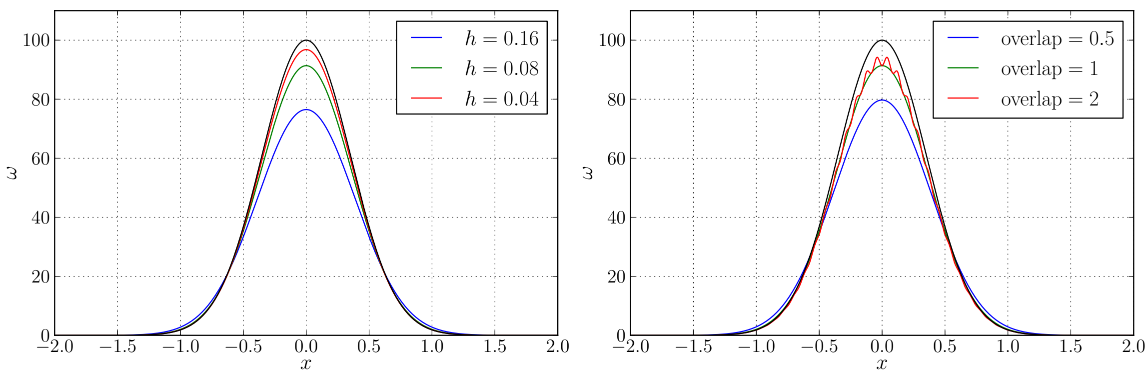

(a) Convergence of h with overlap $= 1.0$ **(b)** Convergence of overlap with $h = 0.08$

Figure 2.6: Convergence of vorticity by modifying the spatial resolution. Figure depicts exact vorticity field ω with [—, black] and various resolutions.

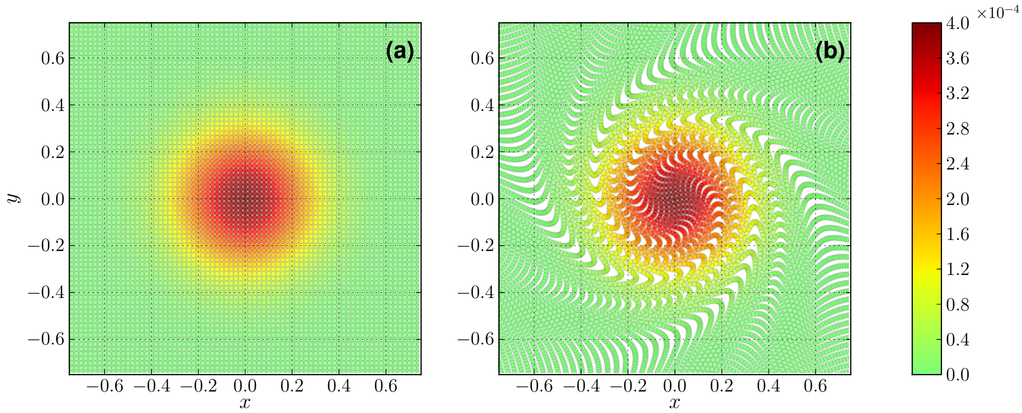

Figure 2.7: Lagrangian distortion of the vortex blobs after 100 steps. The initial vorticity field $\omega(\mathbf{x}, 0) = \exp(-12|\mathbf{x}|)$ with $\Delta t = 0.1$, $\sigma = 0.02$ and overlap $= 1.0$. Figure depicts the initial and the final distribution of the vortex blobs.

the exact vorticity field ω by reducing the nominal particle spacing h. The blobs have overlap $= 1$ and so the blob core-size σ is equal to h. We see that as you reduce the size of the blob and increase the number of particles, the mollified vorticity converges to the exact vorticity. Therefore, an alternate method of reducing the gaussian blurring is to increase the spatial resolution.

Furthermore, we could also adjust the overlap of the blobs, figure 2.6b. The σ and h of the blob is 0.08 and we see that increasing overlap number (i.e reducing the overlap), helps us to recover the original vorticity field. However, as explained by Koumoutsakos [4], if the overlap is too low, we lose the smooth recovery of the vorticity field. This is apparent when overlap $= 2.0$, where we see that the mollified vorticity field is fluctuation.

Therefore, for the hybrid coupling, we set overlap $= 1.0$ and maximize the spatial resolution at the coupling zone.

2.2.6 Remeshing scheme: Treating lagrangian grid distortion

During the convection step, we see that another source of error in the vorticity field is the lagrangian grid distortion. As we have seen before, when the vortex blobs fails to overlap, we are no longer able to reconstruct the correct the vorticity field, figure 2.6b. During the convection, due to the high strains in the fluid, the vortex blobs tent to clump together and creates regions where no vortex blobs are found, reducing the overlap of the blobs, figure 2.7.

We see that due to clustering of the vortex blobs, it fails to reproduce the correct vorticity field. A common strategy to overcome this problem is to remesh the vortex blobs to a uniform grid, so that we have a continuous vorticity field.

However, when transfering the vorticity from the old deformed grid to the new lagrangian uniform grid, we must satisfy the conservation laws of vorticity field. The interpolation methods is based on the conservation of linear impulse which directly implies the

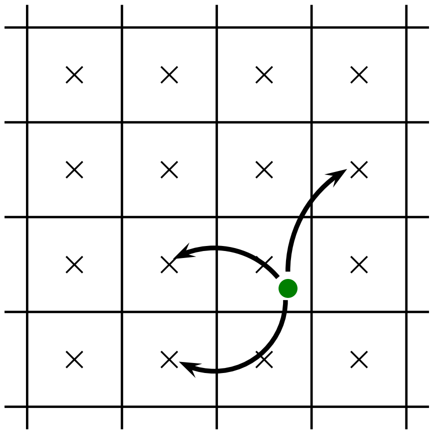

Figure 2.8: Interpolation of vortex blob (•, green) on the uniform grid.

conservation of the total circulation [4]. The transfer of the particle strengths is given as,

$$\alpha_p = \sum_q \tilde{\alpha}_q W\left(\frac{x_p - \tilde{x}_q}{h}\right), \tag{2.25}$$

where the strengths of the particles $\tilde{\alpha}_q$ of the distorted lagrangian grid $\tilde{x}_q$ is transfered to the regular lagrangian grid x_p using the interpolation kernel, weighted W, giving us the remeshing particle strengths α_p. The transfer of strengths of one particles to it's interpolation nodes can be seen in figure 2.8.

M_4' interpolation kernel

For lagrangian problem, we use the efficient interpolation kernel that has been used to reconstruct a smooth distribution interpolation, the M_4' interpolation kernel, introduced by Monaghan [8]. In one dimension it is given as,

$$\mathrm{M'}_4(\xi) = \begin{cases} 1 - \frac{5\xi^2}{2} + \frac{3|\xi|^3}{2} & |\xi| < 1, \\ \frac{1}{2}(2-|\xi|)^2(1-|\xi|) & 1 \leq |\xi| < 2, \\ 0 & 2 \leq |\xi|, \end{cases} \tag{2.26}$$

where $\xi = x_p - x$ is the distance of the particle to the interpolation nodes. The $\mathrm{M'}_4$ is a third-order accurate piecewise smooth B-spline kernel, where $m = 4$ giving it 4 support nodes, figure 2.9. For the two dimensional problem that we have, the 2-D interpolation formula is simply tensor product of the 1-D interpolation kernel equation 2.26, and results in $4^2 = 16$ support nodes, figure 2.8.

The interpolation kernel achieves the third-order accuracy as it also conserves the linear and the angular momentum of the vortex. Koumoutsakos [7] has investigated the drawback of the employing the remeshing strategy and have shown that there is approximately

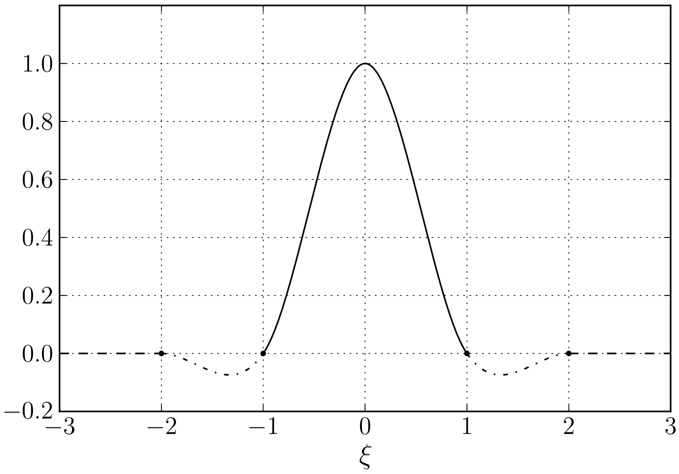

Figure 2.9: Interpolation kernel

4% decay in enstrophy of the flow due to sub-grid dissipation. Note that enstrophy $\mathcal{E}$, is defined as

$$\mathcal{E} = \frac{1}{2}\int_S \omega^2 dS \tag{2.27}$$

and is directly related to the energy (kinetic energy) of the fluid and gives and insight in the energy production and the dissipation of the fluid. Enstrophy is especially useful in turbulence flow investigation as it helps describe the energy cascade of the fluid.

2.3 Diffusion of Vortex Methods

So far, we have dealth with unbounded Euler flow, where we disregarded the viscosity of the flow. However, for real flow we must take in account of the diffusion of the vorticity. Chorin's approach to deal with the viscous term was to employ the viscous splitting algorithm. The flow is segregated to inviscid and viscous component and during the second sub-step we deal with the diffusion of the vorticity, equation 2.7. The equation can again be solved as a system of ODEs, similar to the convection step, where we say,

$$\frac{\mathrm{d}\mathbf{x}_p}{\mathrm{d}t} = 0, \tag{2.28}$$

with

$$\frac{\mathrm{d}\alpha_p}{\mathrm{d}t} = \nu \Delta \alpha_p. \tag{2.29}$$

Therefore in the diffusive step, we fix the position of the vortex blobs and only have to modify the strengths of the particles to mimic the diffusion process. Chorin initially employed a random walk method, which generates and disperse vorticity using pseudo-random number algorithm [3]. However, this method suffers some limitations in accuracy. Since then Particle Strength Exchange (PSE) method [5], has been a common approach that has been used to treat diffusion.

Particle Strength Exchange

The Particle Strength Exchange method, first proposed by Mas-Gallic [5], showed that diffusion can be treated for a particle method isotropic and anisotropic viscosity by approximating the diffusion operator (laplacian) with an integral operator and discretizing the operator using particles. The PSE can be seen as circulation correction method, where during the diffusion step of the viscous splitting algorithm, the strengths of the particle are corrected such that it accounts for the diffusion.

Vortex Redistribution Method

An alternative method to simulate the diffusion is to use the Vortex Redistribution Method (VRM) [9]. The model simulates diffusion by distributing the fraction of circulation of the vortex blobs to each other satisfying the diffusion. The model is based on conserving the moments of the particles by satisfying a linear system of equations. The circulation of the particle are transfer to the nearby particles that are

$$h_\nu = \sqrt{\nu \Delta t_d} \tag{2.30}$$

where h_ν is the diffusion distance and is directly related to the kinematic viscosity ν and the diffusive time-step Δt_d of the simulation. Not that the diffusive time-step Δt_d is equal to the convective time-step Δt_c if the diffusion process is done during every time-step. However, we can easily adjust the diffusion time-step and perform diffusion at a multiple step of the convection.

This is vital as a VRM (and also the PSE) requires a search algorithm to determine the particles that are within the zone of influence. A direct evaluation required $\mathcal{O}\left(N^2\right)$ evaluation, however can be speed up to $\mathcal{O}\left(\log N\right)$ using search tree algorithm.

2.3.1 Modified remeshing for treating diffusion

From further investigation of the VRM, we see that it is similar to remeshing strategy used to counter the lagrangian distortion during the convection process. Therefore Ghoniem and Wee [13] has proposed to combine the remeshing and the diffusion. The application of this methodology was validated by Speck [11]. The diffusion is simulated by the modifying the interpolation kernel of the remeshing process. The key advantage of the modified remeshing method is that now it deals with the uniform remeshing grid helping us eliminating the computational expensive research requirement. The second advantage as shown by the authors is the simplicity. The method only requires a slight modification to the original remeshing tool.

During remeshing, the heat equation is satisfied by transferring the correct fraction of circulation to produce the proper amount of diffusion. The $\mathrm{M'}_4$ kernel was modified to treat the diffusion and is given by:

$$\mathrm{M'}_4(\xi, c) = \begin{cases} 1 - \frac{5\xi^2}{2} + \frac{3|\xi|^3}{2} - c^2\left(2 - 9\xi^2 + 6|\xi|^3\right) & |\xi| < 1, \\ \frac{1}{2}(2 - |\xi|)^2(1 - |\xi|) - c^2(2 - |\xi|)^2(1 - 2|\xi|) & 1 \le |\xi| < 2, \\ 0 & 2 \le |\xi|, \end{cases} \tag{2.31}$$

where

$$c^2 = \frac{\nu \Delta t_d}{h^2}, \tag{2.32}$$

and corresponds to the transfer quantity for diffusion. The addition terms in the interpolation kernel accounts for the diffusion process. When $c \to 0$, the interpolation kernel turns to the classical non-diffusion kernel.

Similar to the VRM, we can perform the remeshing at a given multiple step k_d of the convection step. However, we have an additional constraint on the diffusion time-step Δt_d, equation 2.32. Wee and Ghoniem [13] also investigated the error growth and the stability properties of the interpolation kernel in the Fourier space and have determined that for $\mathrm{M'}_4$ interpolation kernel, we must satisfy

$$\frac{1}{6} \le c^2 \le \frac{1}{2}. \tag{2.33}$$

to ensure amplification factor and the phase error does not grow. This will ensure the stability of the problem and will suppress any spurious oscillations and ensure that it is a non-negative interpolation kernel with non-negative redistribution fractions.

The downside of the this approach, as also for the standard remeshing approach is the global remeshing generates large computation data and scales with the number of particles N. Therefore for problems with large number of particles, a tree-structured remeshing would be more feasible strategy [15].

2.4 Boundary conditions at solid boundary

So far, we have only dealt with unbounded flow. During bounded flow simulation, we must impose addition constraint of the boundary to the simulation to simulate any flow about a geometry. From Helmholtz decomposition, we can have decompose the velocity field to the rotation and the irrotation component, equation 2.8. With the Helmholtz decomposition, we can use the potential component to prescribe the boundary conditions at the solid wall boundary,

$$\mathbf{u}_\phi = \nabla \Phi. \tag{2.34}$$

The incompressibility constraint results in a Laplace's equation for the potential field and unique solution is obtained by enforcing the wall boundary conditions,

$$\mathbf{u}_b \cdot \hat{\mathbf{n}} = (\mathbf{u}_\omega + \nabla \Phi) \cdot \hat{\mathbf{n}}, \tag{2.35}$$

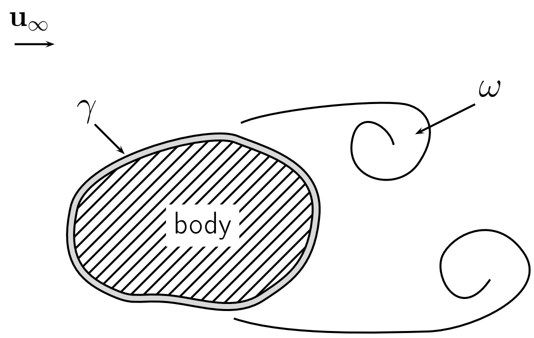

Figure 2.10: Extended vorticity field consisting of vorticity in the fluid and vortex sheet distribution.

and is defined as enforcing the no-through flow at the solid boundary wall, moving at $\mathbf{u}_b$. Note that the $\hat{\mathbf{n}}$ is the normal vector of the solid boundary.

An alternative approach of enforcing the solid boundary condition is not to decompose the velocity field into potential and rotational but to consider the solid boundary as an extension of the vorticity field through vortex sheets, as utilized by Koumoutsakos and Cottet []. Koumoutsakos and Cottet proposed that the bounded problem can be considered as a extended vorticity field consisting of the vorticity in the fluid and the vortex sheet distribution resulted from the tangential velocity discontinuity at the boundary, figure 2.10.

As we have seen in section 2.2, the rotation component $\mathbf{u}_\omega$ represents the vorticity of the flow and to impose the boundary condition of the solid boundary we must deal with the potential component $\mathbf{u}_\phi$. Thus we we will be able to enforce the kinematic boundary condition of the no-through (impermeable) solid boundary.

The Helmholtz decomposition of the velocity flow for bounded flow can be written as

$$\mathbf{u} = \mathbf{u}_\omega + \mathbf{u}_\phi, \tag{2.36}$$

where now, the potential field

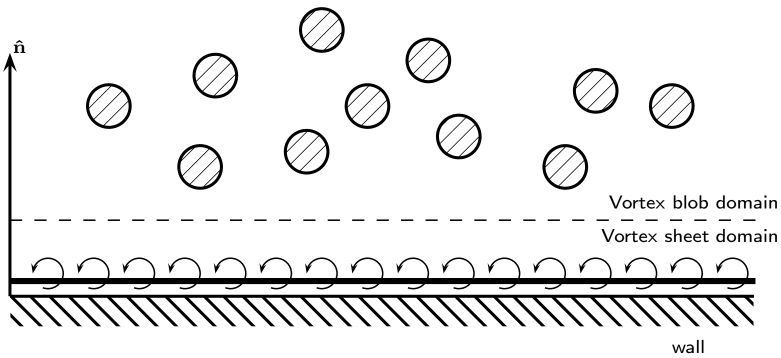

Figure 2.11: Extended vorticity field: Vortex blobs and Vortex sheets

2.4.1 Boundary integral equations

Linked boundary conditions

2.4.2 Panel method for treating no-slip boundary condition

2.4.3 Convergence study of panel method

2.5 Simulation acceleration techniques

2.5.1 Fast multi-pole Method

2.5.2 Parallel computation in GPU

2.6 Validation of lagrangian method

2.6.1 Lamb-oseen vortex at $Re = 100$

2.6.2 Convergence study of the viscous vortex method

2.6.3 Convection of Clercx-Bruneau dipole at $Re = 625$

2.7 Summary

Chapter 3

Eulerian Domain: Finite Element Method

3.1 Introduction to Finite Element Method

3.1.1 Finite element discretization

3.1.2 Finite element function and function space

3.2 Solving the Finite Element problem

3.2.1 Introduction to FEniCS Project

3.2.2 Mesh generation using GMSH

3.3 Solving Incompressible Navier-Stokes Equations

3.3.1 Velocity-pressure formulation

3.3.2 Incremental pressure correction scheme

3.3.3 Determining the vorticity field

3.3.4 Determining the body forces

Frictional Forces

Pressure Forces

3.4 Validation of eulerian method

3.4.1 Clercx-Bruneau dipole collison at $Re = 625$

3.4.2 Impulsively started cylinder at $Re = 550$

3.5 Summary

Chapter 4

Hybrid Eulerian-Lagrangian Vortex Particle Method

4.1 Theory of Domain Decomposition Method

4.1.1 Advantage of domain decomposition

4.1.2 Assumptions and Limitations

4.1.3 Modified coupling strategy

4.2 Eulerian-Lagrangian coupling algorithm

4.2.1 Eulerian dirichlet boundary condition

4.2.2 Vorticity interpolation algorithm

4.3 Introduction to pHyFlow: Hybrid solver

4.3.1 Program structure

4.4 Summary

Chapter 5

Verification and Validation of Hybrid Method

5.1 Error in coupling: Verification with Lamb-Ossen vortex

5.1.1 Generation of artificial vorticity

5.2 Clercx-Bruneau dipole convection at $Re = 625$

5.2.1 Comparison of vorticity contours

5.2.2 Variation in maximum vorticity

5.2.3 Variation in kinetic energy

5.2.4 Variation in enstrophy

5.3 Clercx-Bruneau dipole collison at $Re = 625$

5.3.1 Comparison of vorticity contours

5.3.2 Variation in maximum vorticity

5.3.3 Variation in kinetic energy

5.3.4 Variation in enstrophy

5.3.5 Variation in palinstrophy

5.4 Impulsively started cylinder problem at $Re = 550$

5.4.1 Evolution of the wake

5.4.2 Evolution of pressure and friction drag

5.4.3 Evolution of lift

5.5 Moving body

Chapter 6

Conclusion and Recommendation

6.1 Conclusion

6.1.1 Lagrangian domain

6.1.2 Eulerian domain

6.1.3 Hybrid method

6.2 Recommendations

6.2.1 Lagrangian domain

6.2.2 Eulerian domain

6.2.3 Hybrid method

References

[1] L.a. Barba and Louis F. Rossi. Global field interpolation for particle methods. *Journal of Computational Physics*, 229(4):1292–1310, February 2010.

[2] J.Thomas Beale. On the Accuracy of Vortex Methods at Large Times. In Bjorn Engquist, Andrew Majda, and Mitchell Luskin, editors, *Computational Fluid Dynamics and Reacting Gas Flows SE - 2*, volume 12 of *The IMA Volumes in Mathematics and Its Applications*, pages 19–32. Springer New York, 1988.

[3] AJ Chorin. Numerical study of slightly viscous flow. *Journal of Fluid Mechanics*, 1973.

[4] G H Cottet and P D Koumoutsakos. *Vortex Methods: Theory and Practice*, volume 12. Cambridge University Press, 2000.

[5] S. Degond, P.; Mas-Gallic, Pierre Degond, and S Mas-Gallic. The weighted particle method for convection-diffusion equations. I. The case of an isotropic viscosity. *Mathematics of Computation*, 53(188):485–507, 1989.

[6] CJ Simão Ferreira. The near wake of the VAWT: 2D and 3D views of the VAWT aerodynamics. 2009.

[7] P Koumoutsakos. Inviscid axisymmetrization of an elliptical vortex. *Journal of Computational Physics*, 138(2):821–857, 1997.

[8] J.J Monaghan. Extrapolating B-splines for interpolation. *Journal of Computational Physics*, 60(2):253–262, September 1985.

[9] S. Shankar and L.van Dommelen. A New Diffusion Procedure for Vortex Methods. *Journal of Computational Physics*, 127(1):88–109, August 1996.

[10] Carlos Simão Ferreira, Gijs Kuik, Gerard Bussel, and Fulvio Scarano. Visualization by PIV of dynamic stall on a vertical axis wind turbine. *Experiments in Fluids*, 46(1):97–108, August 2008.

[11] Robert Speck. *Generalized algebraic kernels and multipole expansions for massively parallel vortex particle methods*, volume 7. Forschungszentrum Jülich, 2011.

[12] L.J. Vermeer, J.N. Sø rensen, and a. Crespo. Wind turbine wake aerodynamics. *Progress in Aerospace Sciences*, 39(6-7):467–510, August 2003.

[13] Daehyun Wee and Ahmed F. Ghoniem. Modified interpolation kernels for treating diffusion and remeshing in vortex methods. *Journal of Computational Physics*, 213(1):239–263, March 2006.

[14] Wikipedia. Vertical-Axis Wind Turbine, July 2013.

[15] G S Winckelmans, J K Salmon, Universite Catholique De Louvain, M S Warren, A Leonard, Theoretical Astrophysics, Los Alamos National Laboratories, Los Alamos, B Jodoin, and Universite De Sherbrooke. Application of Fast Parallel and Sequential Tree Codes to Computing Three-Dimensional Flows with the Vortex Element and Boundary Element Methods. 1:225–240, 1996.